Low temperature phase transitions inside CDW phase in kagome metals AV_3Sb_5 (A=Cs,Rb,K): Significance of mixed-type Fermi surface electron correlations

Jianxin Huang[1], Rina Tazai[2], Youichi Yamakawa[1], Seiichiro Onari[1], and Hiroshi Kontani[1]

[1]*Department of Physics, Nagoya University, Nagoya 464-8602, Japan*

[2]*Yukawa Institute for Theoretical Physics, Kyoto University, Kyoto 606-8502, Japan*

(Dated: April 5, 2024)

To understand the multistage phase transitions in V-based kagome metals inside the charge-density-wave (CDW) phase, we focus on the impact of the "mixed-type" Fermi surface because it is intact in the CDW state on the "pure-type" Fermi surface. On the mixed-type Fermi surface, moderate spin correlations develop, and we reveal that uniform ($\boldsymbol{q} = \boldsymbol{0}$) bond order is caused by the paramagnon interference mechanism, which is described by the Aslamazov-Larkin vertex correction. A dominant solution is the E_{2g}-symmetry nematic order, in which the director can be rotated arbitrarily. In addition, we obtain the A_{1g}-symmetry order, which leads to the change in the lattice constants without symmetry breaking. The predicted E_{2g} and A_{1g} channel fluctuations at $\boldsymbol{q} = \boldsymbol{0}$ can be observed by the elastoresistance measurements. These results are useful to understand the multistage phase transitions inside the 2×2 CDW phase. The present theory has a general significance because mixed-type Fermi Surfaces (with multiorbital van-Hove singularities) exist in various kagome lattice systems.

Introduction— Exotic electronic states and correlation-driven superconductivity in kagome metals AV_3Sb_5 (A=K, Cs, and Rb) have attracted increasing attention. Strong Coulomb interaction and the geometrical frustration of V site electrons (in Fig. 1(a)) give rise to exotic quantum phase transition without magnetization. At ambient pressure ($P = 0$), AV_3Sb_5 exhibits 2×2 bond-order (BO) at $T_{BO} = 78, 94$ and 102 K for A=K, Cs and Rb, respectively [1–5]. The BO is the correlation-driven modulation of the hopping integrals (δt_{ij}) (Fig. 1(b)). The superconducting (SC) state appears at $T_c = 1 \sim 3K$ inside the BO phase [6, 7]. Under pressure, T_{BO} gradually decreases, while T_c exhibits non-monotonic pressure dependence [8]. The maximum T_c (~ 10K) is realized around the BO critical pressure $P_c^{BO} \approx 2$GPa, consistently with the BO fluctuation pairing mechanism proposed in Ref. [9]. The predicted s-wave superconductivity has been recently confirmed by the penetration depth and electron irradiation measurements [10, 11].

Rich symmetry-breaking states "inside the BO phase" have been a significant open problem. For example, the C_6 symmetry-breaking nematic state [12, 13] and the time-reversal-symmetry breaking (TRSB) without spin order [4, 14–18] have been reported. These states are caused by the correlation-driven hopping integral modulation: δt_{ij}. The nematic order is given by the bond order with real δt_{ij}, and the TRSB order is given by the imaginary δt_{ij}. The latter accompanies topological charge-current [19] that gives the giant anomalous Hall effect (AHE) [20, 21]. Theoretically, sizable off-site (beyond-mean-field) interaction [9, 22–46] leads to non-local order parameters ($\delta t_{ij} \neq 0$) in kagome metals.

At present, the possible onset temperatures of symmetry-breaking states "inside the BO phase" are unsolved. One possible state, the TRSB order parameter strongly develops below $T^* = 35 \sim 50$K in the μ-SR [14, 16–18] and the AHE [20, 21] measurements. As for another possibility, the nematic state, the scanning birefringence study [13] reports $T_{nem} \approx T_{BO}$, while $T_{nem} \approx 35$K is reported by the elastoresistance measurement [12]. This discrepancy may indicate that the BO layer stacking with π-shift leads to the weak nematicity at T_{BO}, and another nematic order emerges inside the BO phase. The origin of the latter nematicity is not understood at present.

In V-based kagome metals, two major Fermi surfaces (FSs) are composed of the b_{3g}-orbitals and the b_{2g}-orbitals (Fig. 1(a)). The bandstructure and the FSs are shown in Figs. 1(c) and (d), respectively. Both FSs give large density-of-states (DOS) at the Fermi level due to the van-Hove singularity (vHS) at three M points. Near the Fermi level, the b_{3g}-orbital FS is called the "pure-FS", where each vHS point is composed of a single sublattice; see Fig. 1(e). The vHS points are gapped by the 2×2 BO on the pure-FS below T_{BO}; see the unfolded FS in Fig. 1(d). Previous theories have mainly been devoted to understand the significant roles of the pure-type FS [9, 35–37] except for Refs. [41, 43]. However, one may expect that an additional phase transition below T_{BO} would occur on the b_{2g}-orbital FS, the mixed-type FS because it is not harmed by the BO. Its sublattice weight is shown in Fig. 1(f), In addition, it is notable that the mixed-type FS universally exists in usual kagome lattice models. Therefore, the research on the mixed-type FS is of great significance.

In this paper, to understand the phase transitions below T_{BO} in AV_3Sb_5, we focus on the impact of the mixed-type FS because it is intact in the BO phase. On the mixed-type FS, moderate antiferromagnetic (AFM) spin correlations develop, which leads to the uniform ($\boldsymbol{q} = \boldsymbol{0}$) bond order by the paramagnon interference mechanism. This beyond-mean-field mechanism is described by the

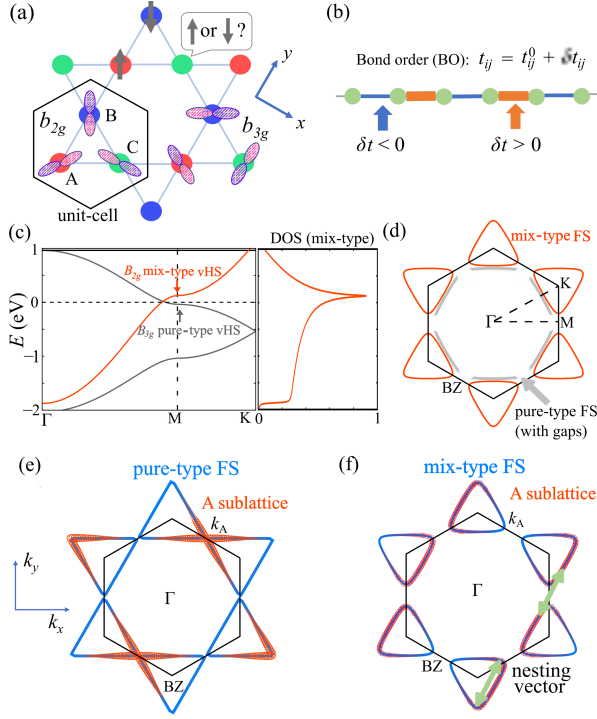FIG. 1. (a) Kagome lattice structure. b_{3g}- and b_{2g}-orbitals are shown. (b) BO parameter given by the hopping integral modulation δt_{ij}. (c) b_{3g}-orbital (with pure-type vHS) and b_{2g}-orbital (with mixed-type vHS) band structure the DOS. (d) FSs of pure-type FS ($n^{\text{pure}} = 2.6$) and mixed-type FS ($n^{\text{mix}} = 1.6$). Here, the pure-type FS exhibits the 2×2 BO induced gap. (e) A-sublattice weight shown by red color on the pure-type FS at $n^{\text{pure}}_{\text{vHF}} = 2.5$. The vHS point at $\boldsymbol{k} = \boldsymbol{k}_A$ is composed of A sublattice. (f) A-sublattice weight on the mixed-type FS at $n^{\text{mix}}_{\text{vHF}} = 1.6$. The vHS point at $\boldsymbol{k} = \boldsymbol{k}_A$ is composed of B+C sublattices.

Aslamazov-Larkin (AL) vertex corrections. A dominant BO solution is the E_{2g}-symmetry nematic order in which the director can be rotated arbitrarily. In addition, we obtain the A_{1g}-symmetry bond order which would accompany the change in the lattice constants. These results are useful to understand the multistage phase transitions inside the 2×2 BO phase.

Model Hamiltonian and Formulations.— In this letter, we study the bond-order phase transition mediated by the quantum fluctuations in kagome lattice Hubbard model with a "mixed-type" FS composed of three b_{2g} orbitals. We apply the density-wave (DW) equation method to derive the optimized order parameter (= symmetry-breaking self-energy $\Delta\Sigma$) driven by the beyond-mean-field vertex corrections. In Ref. [9], the present authors studied the $b_{2g}+b_{3g}$ orbital kagome lattice Hubbard model for AV$_3$Sb$_5$, and found that the pure-type FS alone gives the 2×2 BO state. However, the b_{2g} orbital FS can induce different instabilities for $T \ll T_{\text{BO}}$. For this reason, to find the phase transition inside the BO phase, we study the b_{2g} orbital kagome lattice tight-

binding Hubbard model.

The b_{2g} orbitals at sublattices A-C are shown in Fig. 1(a). The corresponding mixed-type FS is shown in Fig. 1(d). The kinetic term of the b_{2g} orbital model is $H_0 = \sum_{\boldsymbol{k},l,m,\sigma} h_{lm}(\boldsymbol{k}) c^\dagger_{\boldsymbol{k},l,\sigma} c_{\boldsymbol{k},m,\sigma}$, where $h_{lm}(\boldsymbol{k})$ is the momentum representation of the nearest-neighbor hopping integral $t_{lm}(r)$, $l,m = $ A, B, C and σ is the spin index. In our study the unit of energy (Coulomb interaction, hopping integral and temperature) is eV. We set the nearest-neighbor hopping integral $t = -0.5$ [9, 35] and put the number of electrons on the mixed-type FS $n^{\text{mix}} = 1.6$. The 3×3 Green function is given as $\hat{G}(\boldsymbol{k}, \epsilon_n) = [(i\epsilon_n + \mu)\hat{1} - \hat{h}(\boldsymbol{k})]^{-1}$, where $\epsilon_n = (2n + 1)\pi T$ is the fermion Matsubara frequency. We also introduce the on-site Coulomb interaction term $H_U = U\sum_{i,l} n_{i,l,\uparrow} n_{i,l,\downarrow}$, where $n_{i,l,\sigma}$ is the electron number at unit cell i.

In the mean-field-level approximation, the spin instability is the most prominent [9]. In the random phase approximation (RPA), spin susceptibility is $\hat{\chi}^s(q) = \hat{\chi}^0(q)(\hat{1} - U\hat{\chi}^0(q))^{-1}$, where $\chi^0_{l,m}(q) = -T\sum_k G_{l,m}(k + q)G_{m,l}(k)$ is the 3×3 irreducible susceptibility matrix and $q \equiv (\boldsymbol{q}, \omega_l = 2\pi Tl)$. The spin susceptibility diverges when the spin Stoner factor α_s, which is defined as the maximum eigenvalue of $U\hat{\chi}^0(q)$, reaches unity. Figure 2(a) shows the spin susceptibility $\chi^s_{A,A}(\boldsymbol{q})$ at $T = 0.02$ and $\alpha_s = 0.97$ ($U = 2.2$). Its maximum peak appears at the nesting of the A-sublattice FS shown in Fig. 1(f). The real-space short-range spin correlation is depicted in Fig. 2(b). In contrast, such AFM spin fluctuations remain small in the pure-type case. The obtained $\chi^s(\boldsymbol{q})$ is used to construct the kernel function of the DW equation, $I^{L,M}_q(k, p)$ in Eq. (1), which is a non-linear function of $\chi^s(\boldsymbol{q})$. We will show that the AFM spin fluctuations in the mixed-type FS give rise to the exotic ferro-bond orders via the AL vertex corrections.
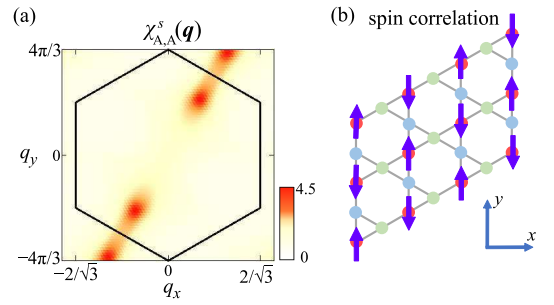

FIG. 2. (a) Obtained $\chi^s_{A,A}(\boldsymbol{q})$ that shows the AFM correlation. (b) Real-space short-range spin correlation.

Density Wave equation analysis.— The nonmagnetic DW orders cannot be obtained by RPA in the Hubbard model with the on-site Coulomb interaction, because the charge Stoner factor α_c is always smaller than spin Stoner factor α_s in mean-field approximation. However, the vertex corrections in the DW equation (Fig 3(a)) give various charge-channel DW states due to the "paramagnon

interference processes".

From a field-theoretical point of view, the nonmagnetic bond-order is described as the symmetry-breaking self-energy $\Delta\Sigma$, which is nothing but the DW order parameter [30]. ($\Delta\Sigma$ is much smaller than the self-energy without symmetry-breaking Σ_0.) Once $\Delta\Sigma$ emerges, it will give the symmetry-breaking in $\chi^0(q) = -T\sum_k G(k+q)G(k)$, where G is the Green function with the total self-energy $\Sigma_{tot}(k) = \Delta\Sigma(k) + \Sigma_0(k)$. In the meanwhile, when symmetry-breaking in $\chi^s(q)$ emerges, the self-energy $\Sigma(k) = \frac{3U^2}{2}T\sum_q \chi^s(q)G(k+q)$ will contain finite $\Delta\Sigma = \Sigma(k) - \Sigma_0(k)$. Such feedback between $\Delta\Sigma$ and $\chi^s(q)$ becomes positive when $\lambda > 1$, so the nonmagnetic bond-order occurs spontaneously. In the DW equation, the form factor describes $\Delta\Sigma$, and the AL terms give the positive feedback effect [47]. This theory was first developed to explain the orbital nematic state in Fe-based superconductors, and it has been applied to the cuprates and the twisted-bilayer graphene successfully [30]. Recently, the BO and current ordered states in kagome metals with pure-type band also have been explained by the AL processes [9, 38].

The DW equation for the charge-channel order is

$$\lambda_q f_q^L(k) = -\frac{T}{N}\sum_{p,M_1,M_2} I_q^{L,M_1}(k,p)$$
$$\times \{G(p)G(p+q)\}^{M_1,M_2} f_q^{M_2}(p), \quad (1)$$

where $I_q^{L,M}(k,p)$ is the "particle-hole (p-h) pairing interaction", the kernel function for charge channel. The detail of it is in the SM A [48]. $k \equiv (\boldsymbol{k}, \epsilon_n)$ and $p \equiv (\boldsymbol{p}, \epsilon_m)$ (ϵ_n, ϵ_m are fermion Matsubara frequencies). $L \equiv (l, l')$ and $M_i \equiv (m_i, m_i')$ represent the pair of sublattice indices A, B, C. λ_q is the eigenvalue that represents the instability of the DW at wavevector q, and $\max_q\{\lambda_q\}$ reaches unity at $T = T_{\mathrm{DW}}$. $f_q^L(k)$ is the Hermitian form factor that is proportional to the p-h condensation $\sum_\sigma\{\langle c_{\boldsymbol{k}+\boldsymbol{q},l,\sigma}^\dagger c_{\boldsymbol{k},l',\sigma}\rangle - \langle\cdots\rangle_0\}$, or equivalently, the symmetry-breaking self-energy $\Delta\Sigma$. In real space, the $\boldsymbol{k}$-dependent form factor gives the correlated hopping between (i, l) and (j, m), which is given as: $\delta t_{il,jm}(= \delta t_{jm,il})^*$.

$$\delta t_{il,jm} = \frac{1}{N}\sum_{\boldsymbol{k}} f_q^{lm}(\boldsymbol{k})e^{i\boldsymbol{k}\cdot(\boldsymbol{r}_{il}-\boldsymbol{r}_{jm})}e^{i\boldsymbol{q}\cdot\boldsymbol{r}_{il}}, \quad (2)$$

where $\boldsymbol{r}_{il}$ represents position of l sublattice in the unit-cell i. The BO preserves the time-reversal-symmetry: $\delta t_{il,jm} = \delta t_{jm,il} = $ real.

The kernel function $I_q^{L,M}$ is given by the functional derivative of the Luttinger ward function $\Phi_{\mathrm{LW}}(G)$. Here, we apply the fluctuation-exchange approximation for $\Phi_{\mathrm{LW}}(G)$. Then, $I_q^{L,M}$ is composed of one Hartree term, one single-magnon exchange Maki-Thompson (MT) term and two double-magnon interference Aslamazov-Larkin (AL) terms, as depicted in Fig. 3(a) [30]. Importantly,

the AL terms represent the "interference between two paramagnons with momenta $\boldsymbol{Q}$ and $\boldsymbol{Q}'$" that leads to the DW order at $\boldsymbol{q} = \boldsymbol{Q} - \boldsymbol{Q}'$; see Fig. 3(b).
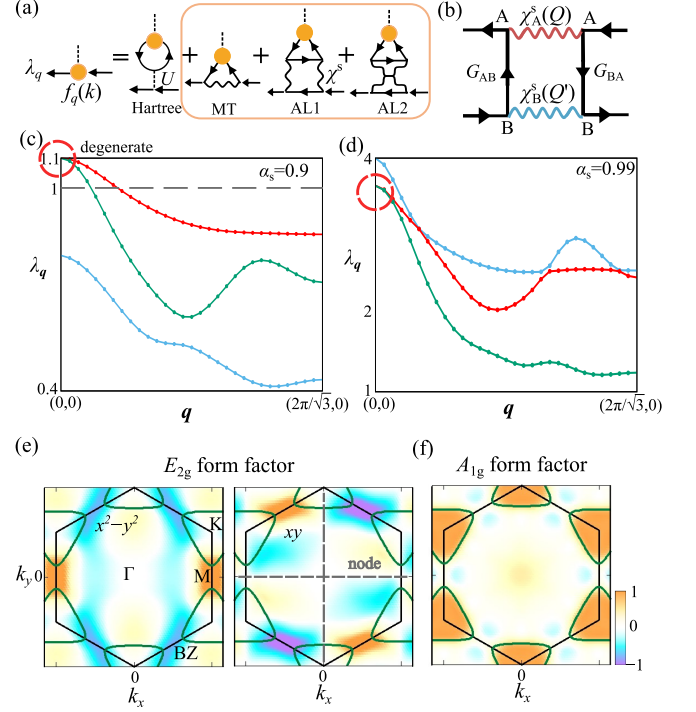

FIG. 3. (a) Linearized DW equation with respect to the form factor $f_q(k)$ and eigenvalue λ_q. The p-h pairing interaction is composed of the Hartree term, the MT term, and the AL terms. The solid line is the non-interacting Green function, and the wave lines are the spin fluctuations from RPA. (b) Interference between two paramagnons ($\boldsymbol{Q}$ and $\boldsymbol{Q}'$) that leads to the DW order at $\boldsymbol{q} = \boldsymbol{Q} - \boldsymbol{Q}'$. (c-d) Eigenvalue λ_q for two cases: (c) Moderate ($\alpha_S = 0.9$) and (d) strong ($\alpha_S = 0.99$) spin fluctuation. Three states are shown in different colors. In both cases, λ_q exhibits the maximum at $\boldsymbol{q} = \boldsymbol{0}$. (e-f) Diagonal form factor $\sum_l^{\mathrm{A,B,C}} f_{\boldsymbol{q}=\boldsymbol{0}}^{ll}(k)$: (e) E_{2g} symmetry solution obtained for $\alpha_S = 0.9$ and (f) A_{1g} symmetry solution obtained for $\alpha_S = 0.99$. Note that off-diagonal form factor is also large.

With the obtained spin susceptibility as the paramagnon, we solve the DW equation. The $\boldsymbol{q}$-dependence of the eigenvalue λ_q at $n^{\mathrm{mix}} = 1.6$ ($T = 0.02$) is exhibited in Figs. 3(c) and (d). (Here, we show λ_q only on the path Γ-M because λ_q on the path M-K-Γ is small.) Figure 3(c) [(d)] shows the result for $\alpha_s = 0.9$ (0.99), where spin fluctuation strength is moderate (strong). Importantly, the maximum peak position is located at $\boldsymbol{q} = \boldsymbol{0}$ in both cases. The obtained $\boldsymbol{q} = \boldsymbol{0}$ order, which is very different from the nesting driven $\boldsymbol{q} \neq \boldsymbol{0}$ order, is naturally derived from the interference between two paramagnons with wavevectors $\boldsymbol{Q}$ and $\boldsymbol{Q}'(= \boldsymbol{Q})$ [30]. For $\alpha_S = 0.9$ in Fig. 3 (c), the largest two eigenvalues are degenerate, and the corresponding form factors are E_{2g} symmetry BO; $(\hat{f}_{x^2-y^2}(k), \hat{f}_{xy}(k))$. The corresponding diagonal

form factor $\sum_l f^{ll}_{q=0}(k)$ is shown in Fig. 3(e). Note that off-diagonal form factors are as large as the diagonal form factors. For $\alpha_S = 0.99$ in Fig. 3(d), the non-degenerate largest eigenvalue corresponds to A_{1g} symmetry form factor shown in Fig. 3(f).

The E_{2g} symmetry BO gives the nematicity, and its director can be rotated at any angle by taking the linear combination of $\hat{f}_{x^2-y^2}(k)$ and $\hat{f}_{xy}(k)$ [25]. To understand the nature of the E_{2g} symmetry nematic state, we discuss the real-space form factor $\delta t_{il,jm}$ based on Eq. (2). When the wavevector is $q = 0$, $\delta t_{il,jm}$ is simply written as $\delta t_{lm}(r)$ with $r \equiv r_{il} - r_{jm}$. The obtained $\delta t_{lm}(r)$ for $f^{lm}_{x^2-y^2}(k)$ at $q = 0$ is shown in Fig. 4(a). (Its schematic picture is given in Fig. 4(b).) It is plotted in two directions (AB and AC) from sublattice A, as a function of the distance R, where the distance between nearest sites is 1. The BO along BC direction is the same as that along AC direction. (The even-parity relation $\delta t_{lm}(R) = \delta t_{ml}(-R)$ is verified.) δt_{ll} at $R = 0$ represents the onsite charge modulation at sublattice l, and δt_{lm} at $R = \pm 1$ ($l \neq m$) represents BO between the nearest sites.

A schematic picture of the hopping modulation due to the nearest BO is given in Fig. 4(c). In this case, the lattice structure will become nematic in the presence of finite electron-phonon coupling due to E_{2g} acoustic mode. We also discuss the FS deformation due to the E_{2g} nematic BO, under the order parameter $H' = \Delta E \sum_{k\sigma} \hat{c}^\dagger_{k\sigma} \hat{f}_\theta(k) \hat{c}_{k\sigma}$, where $\hat{f}_\theta(k) \equiv \cos\theta \hat{f}_{x^2-y^2}(k) + \sin\theta \hat{f}_{xy}(k)$. The ordered nematic FS at $\theta = 0$ with $\Delta E = 0.01$ is showed in Fig. 4(d). By changing the angle θ, the nematic FS can be rotated to any direction.

Another state, the A_{1g} BO, does not break the symmetry of the system. However, it induces the FS deformation due to the hopping modulation and the change in the lattice constants should be accompanied through the finite electron-phonon coupling. In SM B [48], we present the nontrivial hopping modulation caused by the A_{1g} BO.

Figure 4(e) shows the T-dependence of λ for E_{2g} and A_{1g} states, in the case of $U = 1.95$. The obtained λ monotonically increases with decreasing T, while the increment of α_S is moderate (see Fig. 4(f)). Although the obtained transition temperature is relatively high, it will be reduced to below T_{BO} by introducing the self-energy effect [47]. In fact, due to the ordinary self-energy Σ_0 which breaks no symmetry, the Green function is given as $G = 1/(i\epsilon_n - \Sigma_0 - \epsilon_k) \approx z/(i\epsilon_n - z\epsilon_k)$, where the mass-enhancement factor $z^{-1} = m^*/m$ is larger than 1. The factor z leads to the rescaling, $T \to zT$ and $U \to U/z$, under the condition of the fixed α and λ[23]. Thus, the transition temperature will be reduced by z. It is an important future issue to derive a reliable transition temperature by taking account of the self-energy.

In the SM C [48], we discuss the important roles of the AL and MT vertex corrections for the BO. We show that
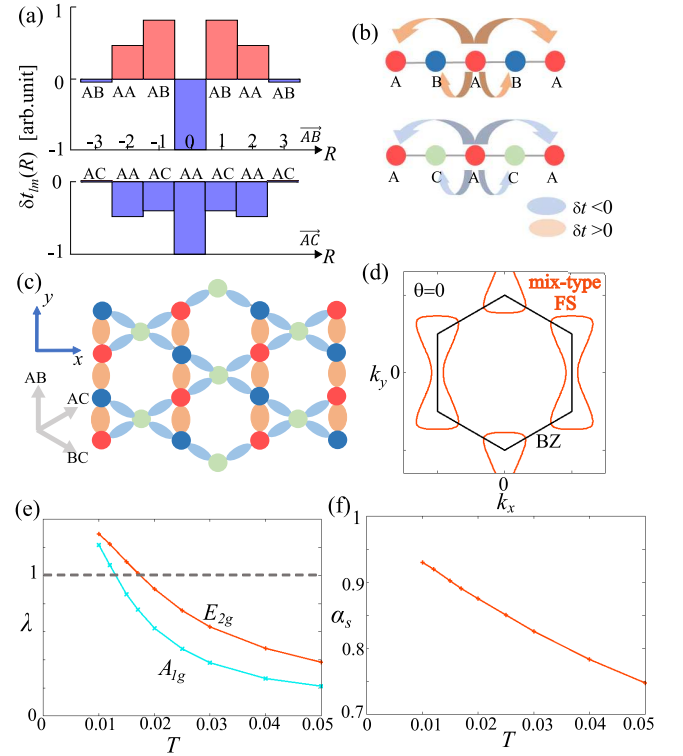

FIG. 4. (a) Obtained $\delta t_{lm}(R)$ along two directions. The horizontal axis means the real space distance. For example, in AB direction, $R = 1$ (2) marks the hopping modulation between the nearest A and B (A and A). Note that $\delta t_{AC}(R) = \delta t_{BC}(R)$. (b) Schematic pictures of $\delta t_{lm}(R)$. (c) Nematic bond order in real space for $\hat{f}_{x^2-y^2}$. Orange color represents $\delta t_{ij} > 0$, while blue color represents $\delta t_{ij} < 0$. (d) Nematic FS induced by the nematic BO $\hat{f}_\theta$. It can be rotated to any angle by changing the angle θ. (e) T-dependence of $\lambda_{q=0}$ for E_{2g} and A_{1g} states, for $U = 1.95$. (f) T-dependence of α_S.

the AL term gives large positive contribution for both E_{2g} and A_{1g} BOs. In addition, it is found that the MT term slightly favors the nodal A_{1g} BO. Interestingly, the same AL process leads to the $q = 0$ BO in mixed-type FS model and 2×2 BO in the pure-type FS model.

Finally, we discuss the results of the existing elastoresistance experiments [49–51] based on the present theory. In Ref. [49], significant E_{2g} symmetry channel nematic correlation is observed under T_{CDW} and above a transition temperature $T_{nem} \sim 35K$. In contrast, in other experiments[50, 51], strong enhancement of A_{1g} channel susceptibility is reported below T_{CDW} and presents a phase transition at $T^* \sim 20K$. Importantly, both E_{2g} and A_{1g} instabilities develop in the mixed-type FS in the present theory, and the leading instability can exchange. Thus, different experimental results may originate from a slight sample dependence. Noteworthy, Ref. [52] reports the nematic order is strongly stabilized under tiny (extrinsic) strain in kagome metal. Thus, the DW equation analysis for the "distorted kagome metal model" would

be useful to understand the variety of the experimental reports. This is an important future issue.

Summary. — We studied the phase transitions below T_{BO} in AV_3Sb_5 by focusing on the mixed-type FS that is intact in the BO phase. It is revealed that the paramagnon interference mechanism leads to the uniform ($\boldsymbol{q} = \boldsymbol{0}$) bond order. A dominant solution is the E_{2g}-symmetry nematic order. We also obtain the A_{1g}-symmetry non-nematic order. These results are useful to understand the multistage phase transitions inside the 2×2 BO phase. This theory has a general significance because mixed-type like multi-sublattice FS exists in many kagome metals, such as ATi_3Bi_5 [53]. In this case, the intra-sublattice nesting gives rise to the AFM spin correlation and such correlation leads to the paramagnon interference. Thus, due to this mechanism, exotic bond orders would occur in various kagome metals.

[1] B. R. Ortiz, L. C. Gomes, J. R. Morey, M. Winiarski, M. Bordelon, J. S. Mangum, I. W. H. Oswald, J. A. Rodriguez-Rivera, J. R. Neilson, S. D. Wilson, E. Ertekin, T. M. McQueen, and E. S. Toberer, *New kagome prototype materials: discovery of* $KV_3Sb_5, RbV_3Sb_5,$ *and* CsV_3Sb_5, Phys. Rev. Materials **3**, 094407 (2019).

[2] B. R. Ortiz, S. M. L. Teicher, Y. Hu, J. L. Zuo, P. M. Sarte, E. C. Schueller, A. M. M. Abeykoon, M. J. Krogstad, S. Rosenkranz, R. Osborn, R. Seshadri, L. Balents, J. He, and S. D. Wilson, CsV_3Sb_5: *A* $\mathbb{Z}_2$ *Topological Kagome Metal with a Superconducting Ground State*, Phys. Rev. Lett. **125**, 247002 (2020).

[3] C. Mu, Q. Yin, Z. Tu, C. Gong, H. Lei, Z. Li, and J. Luo, *S-Wave Superconductivity in Kagome Metal* CsV_3Sb_5 *Revealed by* $^{121/123}Sb$ *NQR and* ^{51}V *NMR Measurements* Chin. Phys. Lett. **38**, 077402 (2021).

[4] Y.-X. Jiang, J.-X. Yin, M. M. Denner, N. Shumiya, B. R. Ortiz, G. Xu, Z. Guguchia, J. He, M. S. Hossain, X. Liu, J. Ruff, L. Kautzsch, S. S. Zhang, G. Chang, I. Belopolski, Q. Zhang, T. A. Cochran, D. Multer, M. Litskevich, Z.-J. Cheng, X. P. Yang, Z. Wang, R. Thomale, T. Neupert, S. D. Wilson, and M. Z. Hasan, *Unconventional chiral charge order in kagome superconductor* KV_3Sb_5, Nat. Mater. **20**, 1353–1357 (2021).

[5] H. Li, H. Zhao, B. R. Ortiz, T. Park, M. Ye, L. Balents, Z. Wang, S. D. Wilson, and I. Zeljkovic, *Rotation symmetry breaking in the normal state of a kagome superconductor* KV_3Sb_5, Nat. Phys. **18**, 265–270 (2022).

[6] B. R. Ortiz, P. M. Sarte, E. M. Kenney, M. J. Graf, S. M. L. Teicher, R. Seshadri, and S. D. Wilson, *Superconductivity in the* $\mathbb{Z}_2$ *kagome metal* KV_3Sb_5, Phys. Rev. Materials **5**, 034801 (2021).

[7] Q. Yin, Z. Tu, C. Gong, Y. Fu, S. Yan, and H. Lei, *Superconductivity and Normal-State Properties of Kagome Metal RbV3Sb5 Single Crystals*, Chin. Phys. Lett. **38**, 037403 (2021).

[8] F. H. Yu, D. H. Ma, W. Z. Zhuo, S. Q. Liu, X. K. Wen, B. Lei, J. J. Ying, and X. H. Chen, *Unusual competition of superconductivity and charge-density-wave state in a compressed topological kagome metal*, Nat. Commun. **12**, 2645 (2021).

[9] R. Tazai, Y. Yamakawa, S. Onari, and H. Kontani, *Mechanism of exotic density-wave and beyond-Migdal unconventional superconductivity in kagome metal* AV_3Sb_5 *(A = K, Rb, Cs)*, Sci. Adv. **8**, eabl4108 (2022).

[10] M. Roppongi, K. Ishihara, Y. Tanaka, K. Ogawa, K. Okada, S. Liu, K. Mukasa, Y. Mizukami, Y. Uwatoko, R. Grasset, M. Konczykowski, B. R. Ortiz, S. D. Wilson, K. Hashimoto, and T. Shibauchi, *Bulk evidence of anisotropic s-wave pairing with no sign change in the kagome superconductor* CsV_3Sb_5, Nat. Commun. **14**, 667 (2023).

[11] W. Zhang, X. Liu, L. Wang, C. W. Tsang, Z. Wang, S. T. Lam, W. Wang, J. Xie, X. Zhou, Y. Zhao, S. Wang, J. Tallon, K. T. Lai, and S. K. Goh, *Nodeless superconductivity in kagome metal* CsV_3Sb_5 *with and without time reversal symmetry breaking*, Nano Lett. **23**, 872 (2023).

[12] L. Nie, K. Sun, W. Ma, D. Song, L. Zheng, Z. Liang, P. Wu, F. Yu, J. Li, M. Shan, D. Zhao, S. Li, B. Kang, Z. Wu, Y. Zhou, K. Liu, Z. Xiang, J. Ying, Z. Wang, T. Wu, and X. Chen, *Charge-density-wave-driven electronic nematicity in a kagome superconductor*, Nature **604**, 59–64 (2022).

[13] Y. Xu, Z. Ni, Y. Liu, B. R. Ortiz, Q. Deng, S. D. Wilson, B. Yan, L. Balents, and L. Wu, *Three-state nematicity and magneto-optical Kerr effect in the charge density waves in kagome superconductors*, Nat. Phys. **18**, 1470 (2022).

[14] L. Yu, C. Wang, Y. Zhang, M. Sander, S. Ni, Z. Lu, S. Ma, Z. Wang, Z. Zhao, H. Chen, K. Jiang, Y. Zhang, H. Yang, F. Zhou, X. Dong, S. L. Johnson, M. J. Graf, J. Hu, H.-J. Gao, and Z. Zhao, *Evidence of a hidden flux phase in the topological kagome metal* CsV_3Sb_5, arXiv:2107.10714

[15] C. Mielke, D. Das, J.-X. Yin, H. Liu, R. Gupta, Y.-X. Jiang, M. Medarde, X. Wu, H. C. Lei, J. Chang, P. Dai, Q. Si, H. Miao, R. Thomale, T. Neupert, Y. Shi, R. Khasanov, M. Z. Hasan, H. Luetkens, and Z. Guguchia, *Time-reversal symmetry-breaking charge order in a kagome superconductor*, Nature **602**, 245–250 (2022).

[16] R. Khasanov, D. Das, R. Gupta, C. Mielke, M. Elender, Q. Yin, Z. Tu, C. Gong, H. Lei, E. T. Ritz, R. M. Fernandes, T. Birol, Z. Guguchia, and H. Luetkens, *Time-reversal symmetry broken by charge order in* CsV_3Sb_5, Phys. Rev. Research **4**, 023244 (2022).

[17] Z. Guguchia, C. Mielke, D. Das, R. Gupta, J.-X. Yin, H. Liu, Q. Yin, M. H. Christensen, Z. Tu, C. Gong, N. Shumiya, M. S. Hossain, T. Gamsakhurdashvili, M. Elender, P. Dai, A. Amato, Y. Shi, H. C. Lei, R. M. Fernandes, M. Z. Hasan, H. Luetkens, and R. Khasanov, *Tunable unconventional kagome superconductivity in charge ordered* RbV_3Sb_5 *and* KV_3Sb_5, Nat. Commun. **14**, 153 (2023).

[18] C. Guo, C. Putzke, S. Konyzheva, X. Huang, M. Gutierrez-Amigo, I. Errea, D. Chen, M. G. Vergniory, C. Felser, M. H. Fischer, T. Neupert, and P. J. W. Moll, *Switchable chiral transport in charge-ordered kagome metal* CsV_3Sb_5, Nature **611**, 461–466 (2022).

[19] F. D. M. Haldane, *Model for a Quantum Hall Effect with-*

out Landau Levels: Condensed-Matter Realization of the "Parity Anomaly", Phys. Rev. Lett. **61**, 2015 (1988).

[20] S.-Y. Yang, Y. Wang, B. R. Ortiz, D. Liu, J. Gayles, E. Derunova, R. Gonzalez-Hernandez, L. Šmejkal, Y. Chen, S. S. P. Parkin, S. D. Wilson, E. S. Toberer, T. McQueen, and M. N. Ali, *Giant, unconventional anomalous Hall effect in the metallic frustrated magnet candidate, KV_3Sb_5*, Sci. Adv. **6**, eabb6003 (2020).

[21] F. H. Yu, T. Wu, Z. Y. Wang, B. Lei, W. Z. Zhuo, J. J. Ying, and X. H. Chen, *Concurrence of anomalous Hall effect and charge density wave in a superconducting topological kagome metal*, Phys. Rev. B **104**, L041103 (2021).

[22] S. Onari and H. Kontani, *Self-consistent Vertex Correction Analysis for Iron-based Superconductors: Mechanism of Coulomb Interaction-Driven Orbital Fluctuations*, Phys. Rev. Lett. **109**, 137001 (2012).

[23] Y. Yamakawa, S. Onari, and H. Kontani, *Nematicity and Magnetism in FeSe and Other Families of Fe-Based Superconductors*, Phys. Rev. X **6**, 021032 (2016).

[24] S. Onari, Y. Yamakawa, and H. Kontani, *Sign-reversing orbital polarization in the nematic phase of FeSe due to the C_2 symmetry-breaking in the self-energy*, Phys. Rev. Lett. **116**, 227001 (2016).

[25] S. Onari and H. Kontani, *SU(4) Valley + Spin Fluctuation Interference Mechanism for Nematic Order in Magic-Angle Twisted Bilayer Graphene: The Impact of Vertex Corrections*, Phys. Rev. Lett. **128**, 066401 (2022).

[26] M. Tsuchiizu, Y. Ohno, S. Onari, and H. Kontani, *Orbital Nematic Instability in the Two-Orbital Hubbard Model: Renormalization-Group + Constrained RPA Analysis*, Phys. Rev. Lett. **111**, 057003 (2013).

[27] M. Tsuchiizu, K. Kawaguchi, Y. Yamakawa, and H. Kontani, *Multistage electronic nematic transitions in cuprate superconductors: A functional-renormalization-group analysis*, Phys. Rev. B **97**, 165131 (2018).

[28] A. V. Chubukov, M. Khodas, and R. M. Fernandes, *Magnetism, Superconductivity, and Spontaneous Orbital Order in Iron-Based Superconductors: Which Comes First and Why?*, Phys. Rev. X **6**, 041045 (2016).

[29] R. M. Fernandes, P. P. Orth, and J. Schmalian, *Intertwined Vestigial Order in Quantum Materials: Nematicity and Beyond*, Annu. Rev. Condens. Matter Phys. **10**, 133 (2019).

[30] H. Kontani, R. Tazai, Y. Yamakawa, and S. Onari, *Unconventional density waves and superconductivities in Fe-based superconductors and other strongly correlated electron systems*, Adv. Phys. **70**, 355 (2023).

[31] R. Tazai, Y. Yamakawa, M. Tsuchiizu, and H. Kontani, *d - and p-wave quantum liquid crystal orders in cuprate superconductors, κ-(BEDT-TTF)$_2$X, and coupled chain Hubbard models: functional-renormalization-group analysis*, J. Phys. Soc. Jpn. **90**, 111012 (2021).

[32] K. Kawaguchi, Y. Yamakawa, M. Tsuchiizu, and H. Kontani, *Competing Unconventional Charge-Density-Wave States in Cuprate Superconductors: Spin-Fluctuation-Driven Mechanism*, J. Phys. Soc. Jpn. 86, 063707 (2017).

[33] Y. Yamakawa and H. Kontani, *Spin-Fluctuation-Driven Nematic Charge-Density-Wave in Cuprate Superconductors: Impact of Aslamazov-Larkin-Type Vertex Correction*, Phys. Rev. Lett. **114**, 257001 (2015).

[34] J. C. S. Davis and D.-H. Lee, *Concepts relating magnetic interactions, intertwined electronic orders, and strongly correlated superconductivity*, Proc. Natl. Acad. Sci. U.S.A. **110**, 17623 (2013).

[35] X. Wu, T. Schwemmer, T. Müller, A. Consiglio, G. Sangiovanni, D. Di Sante, Y. Iqbal, W. Hanke, A. P. Schnyder, M. M. Denner, M. H. Fischer, T. Neupert, and R. Thomale, *Nature of Unconventional Pairing in the Kagome Superconductors AV_3Sb_5 (A = K, Rb, Cs)*, Phys. Rev. Lett. **127**, 177001 (2021).

[36] M. M. Denner, R. Thomale, and T. Neupert, *Analysis of Charge Order in the Kagome Metal AV_3Sb_5 (A = K, Rb, Cs)*, Phys. Rev. Lett. **127**, 217601 (2021).

[37] T. Park, M. Ye, and L. Balents, *Electronic instabilities of kagome metals: Saddle points and Landau theory*, Phys. Rev. B **104**, 035142 (2021).

[38] R. Tazai, Y. Yamakawa and H. Kontani, *Charge-loop current order and Z3 nematicity mediated by bond-order fluctuations in kagome metals*, Nat. Commun. **14**, 7845 (2023).

[39] R. Tazai, Y. Yamakawa and H. Kontani, *Drastic magnetic-field-induced chiral current order and emergent current-bond-field interplay in kagome metals*, Proc. Natl. Acad. of Sci. USA **121**, e2303476121 (2024).

[40] T. Schwemmer, H. Hohmann, M. Durrnagel, J. Potten, J. Beyer, S. Rachel, Y.-M. Wu, S. Raghu, T. Müller, W. Hanke, R. Thomale, *Pair Density Wave Instability in the Kagome Hubbard Model*, arXiv:2302.08517

[41] M. H. Christensen, T. Biro, B. M. Andersen, and R. M. Fernandes, *Loop currents in AV3Sb5 kagome metals: Multipolar and toroidal magnetic orders*, Phys. Rev. B **106**, 144504 (2022)

[42] F. Grandi, A. Consiglio, M. A. Sentef, R. Thomale, and D. M. Kennes, *Theory of nematic charge orders in kagome metals*, Phys. Rev. B **107**, 155131 (2023)

[43] H. D. Scammell, J. Ingham, T. Li, and O. P. Sushkov, *Chiral excitonic order from twofold van Hove singularities in kagome metals*, Nat. Commun. **14**, 605 (2023)

[44] A. Ptok, A. Kobialka, M. Sternik, J. Lazewski, P.T. Jochym, A.M. Oles, and P. Piekarz, *Dynamical study of the origin of the charge density wave in AV_3Sb_5 (A=K, Rb, Cs) compounds*, Phys. Rev. B **105**, 235134 (2022).

[45] H. Kontani, Y. Yamakawa, R. Tazai, and S. Onari, *Odd-parity spin-loop-current order mediated by transverse spin fluctuations in cuprates and related electron systems*, Phys. Rev. Research **3**, 013127 (2021).

[46] R. Tazai and H. Kontani, *Multipole fluctuation theory for heavy fermion systems: Application to multipole orders in CeB_6*, Phys. Rev. B **100**, 241103 (2019).

[47] R. Tazai, S. Matsubara, Y. Yamakawa, S. Onari, and H. Kontani, *Rigorous formalism for unconventional symmetry breaking in Fermi liquid theory and its application to nematicity in FeSe*, Phys. Rev. B **107**, 035137 (2023).

[48] See Supplementary Materials. SM A: Formula of DW equation, SM B: A_{1g} mode, SM C: Important roles of the AL and MT vertex corrections and the quantum interference mechanism.

[49] Y. Sur, K. T. Kim, S. Kim, K. H. Kim, *Optimized superconductivity in the vicinity of a nematic quantum critical point in the kagome superconductor $Cs(V_{1-x}Ti_x)_3Sb_5$*, Nat. Commun. 14, 3899 (2023)

[50] Z. Liu, Y. Shi, Q. Jiang, E. W. Rosenberg, J. M. DeStefano, J. Liu, C. Hu, Y. Zhao, Z. Wang, Y. Yao, D. Graf, P. Dai, J. Yang, X. Xu, J. Chu, *Absence of nematic instability in the kagome metal CsV_3Sb_5*, arxiv:2309.14574

[51] T. Asaba, A. Onishi, Y.Kageyama, T. Kiyosue, K. Ohtsuka, S. Suetsugu, Y. Kohsaka, T. Gaggl, Y. Kasahara, H. Murayama, K. Hashimoto, R.Tazai, H. Kontani, B.

R. Ortiz, S. D. Wilson, Q. Li, H.-H. Wen, T. Shibauchi, and Y. Matsuda, *Evidence for an odd-parity nematic phase above the charge density wave transition in kagome metal CsV_3Sb_5*, arxiv:2309.16985

[52] C. Guo, C. Putzke, S. Konyzheva, X. Huang, M. Gutierrez-Amigo, I. Errea, D. Chen, M. G. Vergniory, C. Felser, M. H. Fischer, T. Neupert, and P. J. W. Moll, *Correlated order at the tipping point in the kagome metal CsV_3Sb_5*, arxiv:2304.00972

[53] J. Huang, Y. Yamakawa, R. Tazai, H. Kontani, *Odd-parity intra-unit-cell bond-order and induced nematicity in kagome metal $CsTi_3Bi_5$ driven by quantum interference mechanism* arxiv:2305.18093

[Supplementary Materials]
Low temperature phase transitions inside CDW phase in kagome metals AV_3Sb_5
(A=Cs,Rb,K): Significance of mixed-type Fermi surface electron correlations

Huang, Jianxin[1], Rina Tazai[2], Youichi Yamakawa[1], Seiichiro Onari[1], and Hiroshi Kontani[1]

[1]*Department of Physics, Nagoya University, Nagoya 464-8602, Japan*
[2]*Yukawa Institute for Theoretical Physics, Kyoto University, Kyoto 606-8502, Japan*

A: Formula of DW equation

We are going to give the formula of the kernel function of the DW equation here. In Eq. (1), the kernel function $I_{\boldsymbol{q}}^{L,M}$ is the irreducible four-point vertex. When $\boldsymbol{q} = 0$, $I_{\boldsymbol{q}}^{L,M}$ is given by the Ward identity: $I_{\boldsymbol{q}}^{L,M} = -\delta\Sigma^L(k)/\delta G^M(k')$, where $L \equiv (l,l')$, $M_i \equiv (m_i, m_i')$ represent the pair of sublattice indices A, B, C. Σ is one-loop fluctuation exchange self-energy. The vertex correction consists of one Hartree term, one single-magnon exchange MT term and two double-magnon interference AL1 and AL2 terms. Their analytic expressions are given as

$$
\begin{aligned}
I_{\boldsymbol{q}}^{l,l',m,m'}(k,k') &= \Gamma_{l,l',m,m'}^c \\
&+ \sum_{b=s,c} \frac{a^b}{2}[V_{l,m;l',m'}^b(k-k') \\
&- T\sum_p \sum_{l_1,l_2,m_1,m_2} V_{l,l_1;m,m_2}^b(p_+)V_{m',m_2;l',l_2}^b(p_-) \\
&\times G_{l_1,l_2}(k-p)G_{m_2,m_1}(k'-p) \\
&- T\sum_p \sum_{l_1,l_2,m_1,m_2} V_{l,l_1;m_2,m'}^b(p_+)V_{m_1,m;l',l_2}^b(p_-) \\
&\times G_{l_1,l_2}(k-p)G_{m_2,m_1}(k'+p)],
\end{aligned} \tag{S1}
$$

where the double-counting in the second order terms should be subtracted. Here $a^{s(c)} = 3(1)$, $p_\pm \equiv p + \boldsymbol{q}/2$, $p = (p, \omega_l)$, and $\hat{V}^b$ is the b-channel interaction matrix given by $\hat{V}^b = \hat{\Gamma}^b + \hat{\Gamma}^b\hat{\chi}^b\hat{\Gamma}^b$. $\hat{\Gamma}^b$ is the b channel bare multiorbital Coulomb interaction. (In the present model, $(\hat{\Gamma})_{ll'mm'}^s = U\delta_{ll'}\delta_{l'm}\delta_{mm'}$ and $(\hat{\Gamma})_{ll'mm'}^c = -U\delta_{ll'}\delta_{l'm}\delta_{mm'}$.) The susceptibility $\hat{\chi}^b(q)$ is given in the main text. The first term in Eq. (S1) is the MT term when the second and third terms are the AL terms. For the higher order term, in the functional-renormalization-group (fRG) study they have been proved unbiased to the DW equation. [26, 27]

B: A_{1g} mode

In the main text, we studied the possible phase transitions in kagome lattice Hubbard model with mixed-type FS by the DW equation. It was found that E_{2g} and A_{1g} symmetry BOs can appear respectively under different spin Stoner factor α_s. The obtained E_{2g} BO form factor and its schematic picture are exhibited in Fig 4. In contrast, the A_{1g} mode breaks no symmetry. Here we explain the obtained A_{1g} symmetry form factor and the corresponding schematic picture. We choose $\alpha_s = 0.975$ ($U = 2.21$ and $T = 0.02$), which is reported in SM B [48] as the transition point for two kinds of BOs.
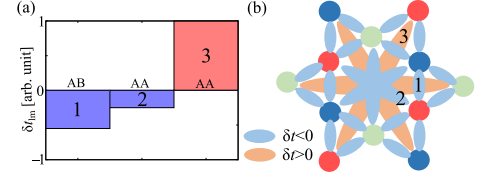

FIG. S1. (a) Main hopping modulations δt_{lm} for A_{1g} mode ($\alpha_s = 0.975, T = 0.02$). The corresponding hopping is in (b). Only hopping modulations related to sublattice A are shown because A_{1g} keeps symmetry. The nearest neighbor hopping and two long-range hoppings are exhibited. (b) Schematic picture of A_{1g} BO, showing two repulsive hoppings and a long-range strong attractive one. The value of the hopping modulation for different number marks are shown in (a) respectively.

As known from Fig. 3(d), the A_{1g} state's maximum eigenvalue also located at $\boldsymbol{q} = 0$. Therefore, the real-space A_{1g} form factor $\delta t_{il,jm}$ becomes intra-unit-cell, like Fig. 4 for the E_{2g} order. The obtained δt_{lm} is exhibited in Fig. S1(a) with the three main values. Fig. S1(a) is the obtained numerical results, showing one nearest neighbor (bond 1) hopping modulation and two long-range (bonds 2 and 3) hopping modulations; see Fig. S1(b). The schematic picture of the obtained A1g order is shown in Fig. S1(b). It can be seen the nearest neighbor hopping reduce. Importantly, long-range hopping modulations δt_{lm} among bonds 2 and 3 emerge irrespective of the fact that the original t_{lm} is zero. These two bonds have opposite sign. Interestingly, the obtained δt_{lm} exhibits the sign-change depending on the distance, and $|\delta t_{lm}|$ is the largest for the next-nearest bonds. These opposite modulations of nearest neighbor hopping and long-range hoppings compete with each others.

Furthermore, the A_{1g} BO will induce the A_{1g} deformation of the FS due to the additional hopping 2 and 3

in Fig. S1(b). In addition, an isotropic lattice deformation will be induced below the A_{1g} BO transition temperature T_{BO}^{A1g} through the finite electron-phonon coupling since the minimum condition of the free energy ($F_{\text{electron}} + F_{\text{lattice}} + F_{\text{electron}-\text{lattice}}$) changes. Importantly, the present theory naturally explains the enhancement of the A_{1g} channel susceptibility observed in Ref. [50] above $T_{\text{BO}}^{A_{1g}}$
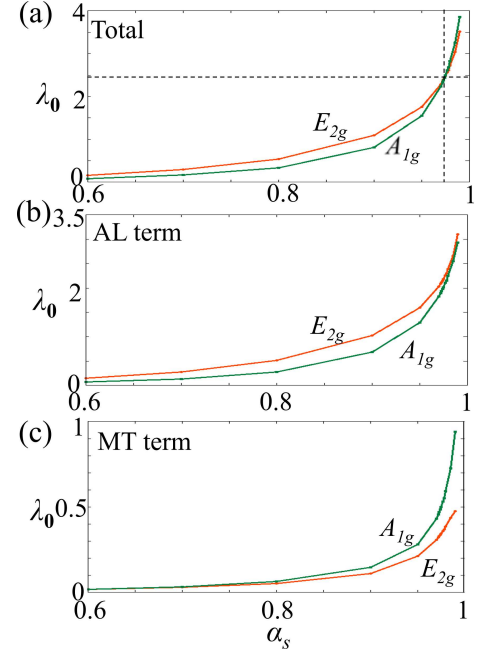

FIG. S2. (a) $\lambda_{\boldsymbol{q}=0}$ for the E_{2g} solution and that for the A_{1g} solution as functions of α_s for $T = 0.02$. These eigenvalues reach unity for $\alpha_S \sim 0.9$. With $\alpha_s \lesssim 0.975$, the E_{2g} solution has the largest λ. For $\alpha_s \gtrsim 0.975$, it is replaced with the A_{1g} solution. (b)(c) Eigenvalue contributed from the AL and MT terms, $\lambda_{\boldsymbol{q}}^{\text{AL}}$ and $\lambda_{\boldsymbol{q}}^{\text{MT}}$, respectively. (Note that $\lambda_{\boldsymbol{q}} = \lambda_{\boldsymbol{q}}^{\text{AL}} + \lambda_{\boldsymbol{q}}^{\text{MT}}$.) While the AL term gives the dominant contribution to $\lambda_{\boldsymbol{q}=0}$, the MT term plays an important role in determining the symmetry and nodal structure of the form factor.

Figures S2 (b) and (c) give the eigenvalue contributed from the AL and MT terms for the fixed form factor, $\lambda_{\boldsymbol{q}}^{\text{AL}}$ and $\lambda_{\boldsymbol{q}}^{\text{MT}}$, respectively. (Note that $\lambda_{\boldsymbol{q}} = \lambda_{\boldsymbol{q}}^{\text{AL}} + \lambda_{\boldsymbol{q}}^{\text{MT}}$.) For both E_{2g} and A_{1g} channels, the AL term gives large positive contribution. In fact, the AL term can stabilize general even-parity BOs, whose wavevector $\boldsymbol{q} = \boldsymbol{Q} - \boldsymbol{Q}'$ (see Fig. 3 (b) in the main text) becomes zero or small (minor) nesting vector [1]. The AL processes give the relation $\lambda_{E_{2g}}^{\text{AL}} \gtrsim \lambda_{A_{1g}}^{\text{AL}}$; see Fig. S2 (b). Thus, the nodal A_{1g} BO originates from the large MT term; see Fig. S2 (c). The A_{1g} BO with $\lambda_{\boldsymbol{q}=0} \sim 1$ will be realized if the self-energy effect reduces the eigenvalue[1].

Finally, we are going to discuss the different BO arose by mixed- and pure-type FS. The quantum interference mechanism produces the nearest site BO in both the mixed-type FS and the pure-type FS models. However, the wavevector is $\boldsymbol{q} = \boldsymbol{0}$ in the mixed-type FS and $\boldsymbol{q} \neq \boldsymbol{0}$ in the pure-type FS. To understand this difference, we focus on the significant role of the vHS points. Since the vHS is composed of two sublattices in the mixed-type FS, the $\boldsymbol{q} = \boldsymbol{0}$ nearest site BO is efficiently realized by the intra-vHS scattering. In contrast, in the pure-type FS, the vHS is composed of a single sublattice, so the inter-site BO should be given by the inter-vHS process at $\boldsymbol{q} = \boldsymbol{q}_{\text{vHS1}} - \boldsymbol{q}_{\text{vHS2}}$. Thus, we can understand the different BOs between both FSs by using the unique present theory.

C: Important Roles of the AL and MT Vertex Corrections and the Quantum Interference Mechanism

Here, we discuss the important roles of the AL and MT vertex corrections for the nematic order. Figure S2 (a) shows the obtained $\lambda_{\boldsymbol{q}=0}$ for the E_{2g} solution and the A_{1g} solution as functions of α_s for $T = 0.02$. These eigenvalues reach unity for $\alpha_S \sim 0.9$. With increasing α_S, the largest eigenvalue state changes from E_{2g} BO to A_{1g} BO at $\alpha_s \sim 0.975$. (Simple charge order is prohibited by the Hartree term.)

[1] H. Kontani, R. Tazai, Y. Yamakawa, and S. Onari, *Un-*